Effect of polyacrylamide friction reducer on calcite dissolution rate at 25 °C and implication for hydraulic fracturing

Yukun Ji [a], Caitlin Walkinshaw [a], Grace Belshaw [a], Veerle Vandeginste [a, b *]

[a] School of Chemistry, University of Nottingham, Nottingham, NG7 2RD, United Kingdom

[b] KU Leuven Campus Bruges, Dept. Materials Engineering, B-8200 Bruges, Belgium

Abstract: Hydraulic fracturing is widely used to create cracks and increase the size and connectivity of existing fractures, leading to higher permeability of shale rocks and production of unconventional hydrocarbon sources. The main chemicals used in hydraulic fracturing fluids can initiate fractures in shale reservoirs by acid induced carbonate dissolution, and minimise energy loss during the pumping process by friction reducer enhanced fluid viscosity. Here, using batch reactor experiments we investigate the effect of non-ionic polyacrylamide polymer (friction reducer) on the dissolution rate of calcite in acidic solutions (0.2 M buffer solution of sodium acetate/acetic acid) at 25 °C. The results demonstrate that polyacrylamide (from 0 to 30 mg) slows down the dissolution rate by a factor of 4. Hydrogen bonding and surface complexation between non-ionic polyacrylamide and calcite potentially trigger an adsorption mechanism that protects calcite from dissolving. This research provides new insights into friction reducer (polyacrylamide) influenced pore generation, enabling engineers to optimise the fracturing fluid design (amount of polyacrylamide) and to consider suitable actions to prevent the polymer from having a negative impact on productivity.

Keywords: polyacrylamide polymer; friction reducer; calcite dissolution; dissolution inhibition.

1 Introduction

Hydraulic fracturing has enabled enhanced recovery of unconventional gas from deep and low permeability shale reservoirs by high pressure injection. The hydraulic fracturing fluid is commonly composed of water, proppant, and various chemicals (King, 2012; Hammack et al., 2014). The additive chemicals (e.g. acid, friction reducer, scale inhibitor, biocide, corrosion inhibitor, and occasionally other additives) are applied to improve the efficiency of the hydraulic fracturing operations (Ferrer and Thurman, 2015). Acids and friction reducers are two of the main constituents of chemical additives in fracturing fluids (Gregory et al., 2011), and they are designed to stimulate the productivity potential by initiating fractures and minimising friction between the fluid and the pipe (Vidic et al., 2013). Acids can dissolve the carbonates (i.e. calcite and dolomite) and create pore space in target shale reservoirs. These dissolution pores act as the nucleation points to trigger further formation and propagation of fractures (Renard et al., 2009), thus exposing an increased contact area between reactive minerals and fracturing fluids and maximising the growth and connectivity of fracture networks. Proppant material (such as sands, resins, or ceramics) holds the induced fractures open, maintaining porosity and allowing gas flow as injection pressure decreases (Gregory et al., 2011; Britt, 2012). The proppant remain

*Corresponding author.
E-mail address: veerle.vandeginste@gmail.com

suspended in the liquid phase by applying a high pumping rate, and friction reducer is therefore introduced in the fracturing fluid to allow a higher pumping rate (Gordalla et al., 2013) and lower pumping cost (Vidic et al., 2013). Friction reducer polymer can decrease the turbulent friction drag by avoiding the formation of a vortex (Sun et al., 2014), thus decreasing friction and promoting laminar flow (Motiee et al., 2016; Yang et al., 2019).

In hydraulic fracturing fluids, high molecular weight (normally over 10^6 Da) polyacrylamide (PAM) (long chain polymer, linear structure) is the most commonly applied friction reducer with high water solubility and good thermal stability (Xiong et al., 2018a; Yang et al., 2019). In Pennsylvania, 100 fracturing operations were randomly selected, and PAM was used in 100% of these fracturing operations (Xiong et al., 2018b). Habibpour and Clark (2017) found that drag reduction rate increases from 30% to 67% with increasing PAM from 100 to 1000 wppm (i.e. parts per million by weight). The PAM polymers can be generally classified into three categories: anionic PAM, cationic PAM, and non-ionic PAM (Carman and Cawiezel, 2007). The polymers utilised in hydraulic fracturing operations depend on the environmental conditions. Anionic PAM have a better performance in a fresh water environment (Sun 2014; Rodvelt et al., 2015), whereas cationic PAM have demonstrated an enhanced performance at high salinity scenario (Rimassa et al., 2009; Nguyen et al., 2018). The potential advantages provided by friction reducer also include reduced chemical usage, fewer environmental concerns, and decreased water consumption (Geri et al., 2019).

Carbonates, quartz, and clay are the main mineral components of shale (Shaw and Weaver, 1965; Chalmers et al., 2012). Different shales are characterised with differing mineralogical compositions. Barnett and Woodford Shales are rich in clays and quartz whereas Haynesville and Eagle Ford Shales are enriched in calcite (Slatt, 2013). Calcite is the main mineral in carbonate-bearing reservoirs, and it is worth to understand the interaction between calcite and fracturing fluids during stimulation. It has proven that the combination of hydraulic fracturing with acidizing is an enhanced stimulation technique to increase the production of the calcite-rich shales (Kharisov et al., 2012; Morsy et al., 2013; Wu and Sharma, 2015; Guo et al., 2017). The formation of high conductivity channels (wormhole) due to acidizing induced mineral dissolution is recognized as an efficient way to increase permeability, and a minor change in porosity can profoundly affect the rock permeability (Gouze and Luquot, 2011; Zou et al., 2018). Calcite can occur embedded into rock matrix or as cements in natural fractures, and the interaction between calcite-bearing shales and acidic fracturing fluid can generate dissolution pores and initiate fractures (Shovkun and Espinoza, 2017). The kinetics of calcite dissolution has been widely investigated under different pH conditions and temperatures, and the calcite dissolution rate increases by increasing solution acidity and increasing temperature (Sjöberg and Rickard, 1984; Chou et al., 1989; Cubillas et al., 2005; Dolgaleva et al., 2005). Three surface reactions occur simultaneously at the solid-fluid interface during calcite dissolution (Sjöberg, 1976; Plummer et al., 1978; Chou et al., 1989; Brown et al., 1993; Fredd and Fogler,

1998):

$$CaCO_3 + H^+ \xleftrightarrow{k_1} Ca^{2+} + HCO_3^- \quad (1)$$

$$CaCO_3 + H_2CO_3^* \xleftrightarrow{k_2} Ca^{2+} + 2HCO_3^- \quad (2)$$

$$CaCO_3 + H_2O \underset{k_4}{\xleftrightarrow{k_3}} Ca^{2+} + HCO_3^- + OH^- \quad (3)$$

Far from equilibrium, the dissolution rate of calcite can be determined as follows:

$$R = k_1 a_{H^+} + k_2 a_{H_2CO_3^*} + k_3 a_{H_2O} - k_4 a_{Ca^{2+}} a_{HCO_3^-} \quad (4)$$

where $H_2CO_3^*$ stands for the sum of dissolved molecular CO_2(aq) and H_2CO_3 in the aqueous solution; the rate constant k_1, k_2, k_3 refer to the above three forward reaction, the rate constant k_4 refers to back-reaction; a_X denotes activities of species X. The dissolution is controlled by H^+ attack (Eq. 1) at low pH when the CO_2 partial pressure is low (i.e. negligible amounts of H_2CO_3) (Fredd and Fogler, 1998). The reaction involving H_2CO_3 becomes significant when pH exceeds 5 and CO_2 pressure exceeds about 0.1 atm (Eq. 2). Calcium precipitation begins to play a role at high pH condition (Eq. 3). In addition, the hydrodynamic conditions are critical for the processes at the calcite-solution boundary and subsequently the dissolution rate. Closer to the sediment-water interface, molecular diffusion dominates the solute transport in the thin water film (termed as the diffusive boundary layer, DBL) (Sulpis et al., 2019). The DBL thickness depends on the roughness of the substrate and the hydrodynamic flow conditions (slower flow velocity produces thicker DBL, and vice versa) (De Baere et al., 2016). Increased flow rate increases the calcite dissolution rate (Gong et al., 2008), but it is not our intent here to simulate real hydrodynamic conditions for calcite dissolution. This study is more about rate comparison between with or without PAM, and thus provides key information on friction reducer (polyacrylamide) influenced calcite dissolution (pore generation) and benefits the design of hydraulic fracturing fluids. Hence, the differences in rates may exist between the laboratory experiments and the technical practices in the field.

It is noted that there are components that can inhibit calcite dissolution, such as Mg^{2+} cations (Compton and Brown., 1994) and phosphate (Berner and Morse, 1974). Mg^{2+} cations can slow the dissolution rate of calcite as a result of Mg^{2+} ions competing with Ca^{2+} ions for adsorption sites on mineral surfaces, thus reducing the empty sites to receive dissolving lattice Ca^{2+} ions (Compton and Brown., 1994). Phosphate acts in a similar way; the retardation effect is attributed to the blocking of active sites by adsorption of phosphate ions at the surface (Berner and Morse, 1974).

Many of the previous studies on kinetic dissolution of calcite have focused on pH effect and/or the foreign ions effects. However, the PAM effect on the dissolution rate of calcite has not been well documented. The aim of our study is to study the dissolution rate of calcite in fluids with different PAM mass by kinetic tests. The results obtained will

provide new insights into fracture initiation in calcite-bearing shale reservoirs in the presence of friction reducer (PAM) during on-going fracturing operations to optimise the fracturing fluid design.

2 Methodology

2.1 Sample preparation

The starting material is Iceland spar optical calcite crystals sourced from Mexico. The calcite crystal was ground to a fine powder with an agate pestle and mortar, and then sieved to obtain a grain size of 63-125 μm. The calcite powder was ultrasonically cleaned in deionised water until the supernatant liquid was clear. The calcite was then dried in a drying oven for three days at 50 °C. This calcite powder was subsequently used in the batch reactor experiments.

2.2 Calcite dissolution batch reactor experiments

Dissolution experiments were conducted in 250 mL batch reactors, and all experiments were carried out using 2.0 g of calcite in 200 mL of simulated fracturing fluids. The non-ionic PAM polymer was used as the friction reducer in our batch reactor experiments. The first trial of our experiments involved using 160 μL hydrochloric acid (12 M) prepared to simulate fracturing fluids (starting pH of 2).

In the experiment that did not contain non-ionic PAM, an initially large increase in pH was observed when calcite powder dissolved in hydrochloric acid (Fig. 1). However, the pH slowly increased in the trial using 20 mg of non-ionic PAM (Fig. 1). Hence, the rates for the experiments that did not contain PAM, can be derived at circumneutral pH conditions, whereas the PAM-containing experimental calcite dissolution rates can be derived in more acidic conditions for the most part (Fig. 1). In order to reliably compare the rates between the PAM-containing experiments and the PAM free experiments, the pH conditions should be controlled using a buffer solution. In addition, it is important to choose a suitable buffer solution. Buffer solution contains phosphate should be avoided since it is a known inhibitor for calcite dissolution. Citric acid should be avoided as well since it will chelate with calcium (Mohan, 2003).

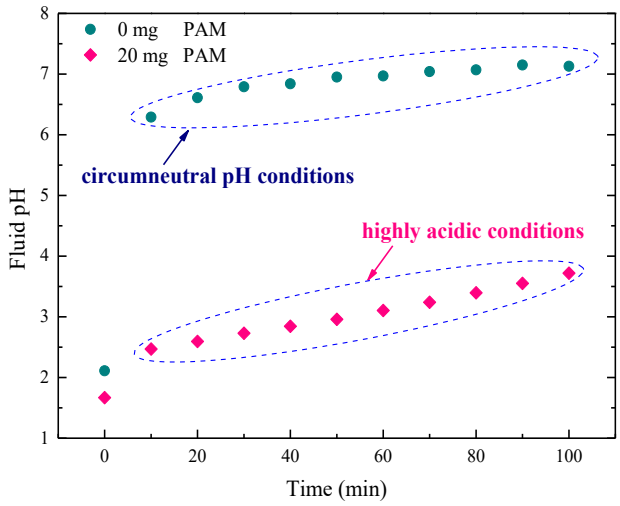

Fig. 1. pH variation as a function of time for experiments with and without non-ionic PAM polymer (Hydrochloric acid trial).

A fixed ratio of 0.2 M sodium acetate and 0.2 M acetic acid buffer solution is used to simulate the acidic fracturing fluid and a starting fluid pH of 4.6 is obtained. A buffer solution was used in numerous mineral dissolution experiments (Wolff-Boenisch and Traina, 2007; Roncal-Herrero and Oelkers, 2011; Farhang et al., 2017). Given that we used the same buffer-solution concentration in the experiments, we can make a comparison of the dissolution rates of calcite in fluids with different PAM mass. Moreover, rates generated in this study are similar to those obtained in buffer free solution (see discussion in section 4). The experimental results from Fredd and Fogler (1998) showed that no significant acetate adsorption occurs on calcite and complex formation does not influence a limiting step of the dissolution mechanism. The non-ionic PAM polymer was then dissolved in this buffer solution (200 mL), and the polymer mass experiments (0, 10, 20, 25, and 30 mg) were conducted to investigate the impact of polymer on the dissolution rate of calcite. It was found that the polymer did not fully dissolve at 25 °C, and it was dissolved in the solution at 45 °C. After complete dissolution, the solution was cooled down to 25 °C.

Each calcite powder (2.0 g) was added to a 200 mL solution in a closed batch reactor placed on a hot plate stirrer, where the suspension was continuously stirred using a Teflon-coated magnetic stirrer bar. Each experiment was run for a total of 100 minutes, and aliquots (1.5 mL) were sampled every ten minutes up to 100 minutes and filtered through 0.45 μm polyethersulfone (PES) membranes for further analysis (0.22 μm filter was not used since the solution was very viscous). One mL of fluid was extracted, acidified and diluted 10 times in an ultrapure HNO_3 (2%) matrix to measure calcium concentration using inductively coupled plasma optical emission spectroscopy (ICP-OES). Fluid pH was measured using an in-situ pH meter placed inside the batch reactor (Fig. A.1 in Appendix A). All experiments were duplicated. The results enable quantification of the calcium mobilisation under different experimental scenarios, thus establishing the impact of PAM on the dissolution of calcite.

2.3 Analytical methods

The BET (Brunauer Emmett Teller) specific surface area of the non-reacted calcite powder was measured using 5-point N_2 adsorption isotherms with a Micromeritics 3Flex surface area analyzer, degassing the sample with nitrogen for 12 h at 100 °C. The specific surface area was 0.26±10% $m^2 \cdot g^{-1}$.

ICP-OES analyses were carried out to quantitatively evaluate the calcium concentration in the sampled fluids from the batch reactor experiments over eleven time steps by using a Perkin Elmer spectrometer Optima 2000 DV. A standard solution containing 28 elements (Fisher Chemicals, 100 mg/L) was used to make a calibration series of 0.1, 1, 3, 5, 7, and 10 mg/L solutions with 2% ultrapure HNO_3 matrix.

2.4 The calculation of calcite dissolution rate

In the batch reactors, the calcite dissolution rate is calculated from the change in concentration of calcium over time, the total calcite surface area, the volume of the fluid in the reactor, and the stoichiometric factor of Ca in calcite ($CaCO_3$). During the dissolution of calcite, the fluid chemistry is influenced by the mobilisation of calcium in solution, as well as an increase in pH. The decrease in calcite mass over time is calculated, as well as the change in total and specific surface area and variation in fluid volume by sample collection. The total calcite surface area is determined by the specific surface area ($m^2 \cdot g^{-1}$) multiplied by the remnant mass of calcite powder (g). A quasi-spherical rough particle shape is assumed to calculate the increase in specific surface area as dissolution proceeds. The calculations are presented in Appendix B. Given that dissolution of calcite in the slightly acidic solution is initially fast (calcite losses are 39% and 45% of the initial mass of the starting material after 10 minutes and 20 minutes reaction time, respectively), the calcite dissolution rate is calculated from the differences in Ca concentration in steps of 10-minute intervals (in the range of 30-80 minutes, six data points). The resulting average dissolution rate in each experiment is used to evaluate the PAM effect on the calcite dissolution rate. The average pH and standard deviation of pH used for the dissolution rate determination are calculated, yielding a pH standard deviation of less than 0.14. The calculation of the calcite dissolution rate is given as:

$$R = \frac{\mathrm{d}C}{\mathrm{d}t} \cdot \frac{V}{NA_c} \tag{5}$$

where R is the dissolution rate ($mol \cdot m^{-2} \cdot s^{-1}$), C denotes concentration ($mol \cdot L^{-1}$), t is time (s), V stands for the fluid volume in the reactor (L), A_c is the total surface area of the sample (m^2), and N denotes the stoichiometric factor of Ca.

3 Results

3.1 Non-ionic PAM polymer influenced pH variation

Batch experiments were carried out to investigate the interaction of calcite with simulated fracturing fluids that contained different polymer mass. The pH of the buffer solutions (0.2 M sodium acetate and 0.2 M acetic acid) with dissolved polymers was 4.6 to simulate the slightly acidic fracturing fluid (Fig. 2). In the first 10 minutes of the 0 mg polymer experiment, solution pH increased from 4.6 to 4.9 given the buffer control of the solution. Moreover, the fluid pH throughout the experiments was slightly acidic regardless of the polymer mass. The experimental results show that pH slightly increased with time, and a faster increase in pH occurred in the first 10 minutes followed by a more gentle increase (Fig. 2). Furthermore, the results demonstrate that an elevated polymer mass leads to a smaller increase in fluid pH, and the final fluid pH varies from 5.4 (0 mg polymer) to 4.9 (30 mg polymer) with increasing amount of polymer.

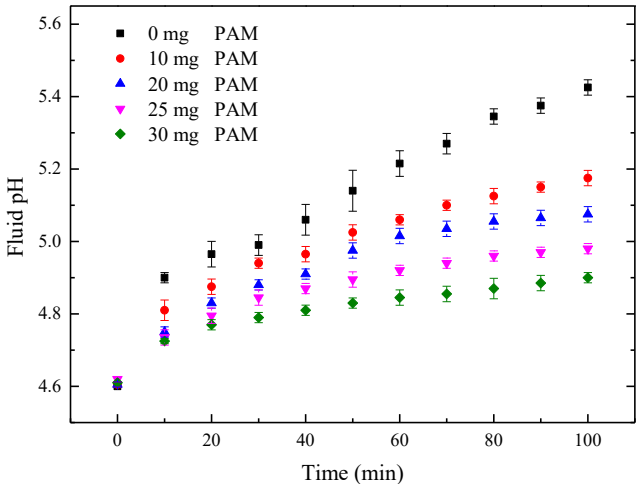

166

167 **Fig. 2.** pH variation in a series of buffer solutions with different PAM mass during calcite dissolution.

168 **3.2 Kinetics of calcite dissolution in non-ionic PAM-containing acidic buffer solutions**

169 The concentration of calcium in the batch reactor experiments increased with time, with a fast increase within the
170 first 10 minutes, followed by a slower increase (Fig. 3). The largest calcium concentration (3155 mg/L) was observed for
171 the experiment that did not contain polymer whereas the highest amount of polymer (30 mg) caused the lowest
172 concentration of calcium (1302 mg/L). At the end of the experiments, 78.8%, 59.6%, 50.8%, 40.3% and 32.5% of the
173 calcite starting material was dissolved in the experiments with 0, 10, 20, 25, and 30 mg polymer, respectively (Fig. 3).
174 Moreover, it should be noted that the calcium concentration is lower (e.g. experiment No. 5 in Fig. 3) in the experiments
175 with lower pH (e.g. experiment No. 5 in Fig. 2). The calcite dissolution rate is thus opposed to the expected effect of pH,
176 thus suggesting that non-ionic PAM polymer decreases the amount of dissolved calcite over a certain length of time and
177 retards calcite dissolution.

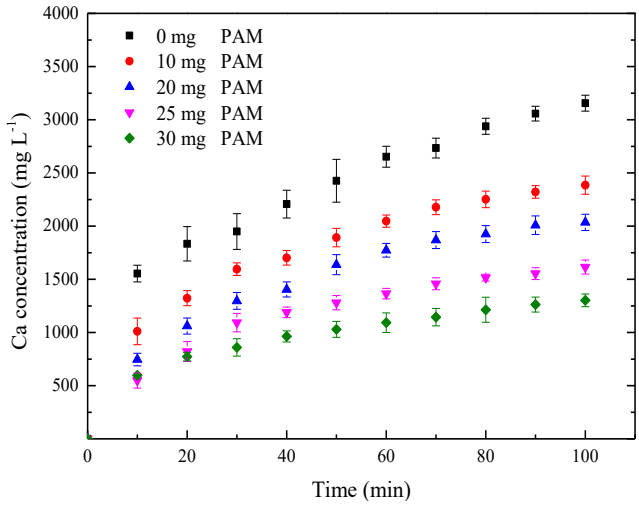

178

179 **Fig. 3.** Variation in calcium concentration as a function of time for the experiments with different amount of non-ionic PAM polymer.

180 Surface free energy could be defined as the excess energy at the material surface compared with its bulk (e.g. Allain
181 and Echeverry-Rendón, 2018). Surface atoms always have higher energy than atoms in the bulk of the material since

182 atoms at the surface are under-coordinated and have strongly asymmetric bonding configurations (atoms at the surface
183 of a material can only bond with the atoms next to them and underneath them) compared with interior atoms (Konhauser,
184 2007). Sample preparation by crushing or grinding could produce structurally damaged surface (fresh surface) (Pracný
185 et al. 2019), and the surface free energy of these particles helps to destabilize them compared to the bulk material (higher
186 reactivity) (Holdren Jr and Berner, 1979). The initial increase in Ca-concentration has been generally attributed to a fast
187 dissolution of ultrafine particles (high surface free energy) (Holdren Jr and Berner, 1979), and the determined values of
188 the dissolution rates at the beginning of the experiment could be overestimated. Therefore, the rate of calcite dissolution
189 (Table 1) in the simulated fracturing fluids was derived by taking into account the 30 to 80 minutes interval of reaction.
190 In the experiment used to calculate the calcite dissolution rate, the pH value was the average pH calculated with six pH
191 measurements in the 30-80 min interval (Table 1). The rate of dissolution of calcite (Eq. 5) at each time point is determined
192 from the difference in Ca concentration in 10-minute intervals as explained above. The average calcite dissolution rate
193 decreases for a lower fluid pH scenario, varying from 5.3×10^{-6} $mol\cdot m^{-2}\cdot s^{-1}$ at pH of 5.2 to 1.3×10^{-6} $mol\cdot m^{-2}\cdot s^{-1}$ at fluid
194 pH of 4.8 (Table 1). This demonstrates that the decrease in dissolution rate is not caused by the effect of pH, but by the
195 effect of PAM. Furthermore, calcite dissolution rates are commonly of an order of 10^{-6} $mol\cdot m^{-2}\cdot s^{-1}$ at a pH of 5 (e.g.
196 Cubillas et al., 2005). This means the rates in our study are reasonable for the pH of around 5 and 25 °C.

197 **Table 1** Average calcite dissolution rates calculated based on the experiments with non-ionic PAM containing-solution. The pH value is the
198 average pH (± stdev) calculated from six pH measurements (30-80 min) in the experiment used to calculate the calcite dissolution rate.

No.	Starting material	PAM mass (mg)	pH	Rate ($mol\cdot m^{-2}\cdot s^{-1}$)
1	calcite	0	5.17±0.14	$5.3\times10^{-6}\pm1.6\times10^{-6}$
2	calcite	10	5.04±0.07	$3.0\times10^{-6}\pm9.4\times10^{-7}$
3	calcite	20	4.98±0.07	$2.6\times10^{-6}\pm1.3\times10^{-6}$
4	calcite	25	4.91±0.04	$1.6\times10^{-6}\pm2.9\times10^{-7}$
5	calcite	30	4.83±0.03	$1.3\times10^{-6}\pm3.5\times10^{-7}$

199 The addition of PAM resulted in a decrease in calcite dissolution rate (Fig. 4). The rates of the two highest PAM
200 concentrations are significantly lower than the rates of the two lowest concentrations as they fall outside of the error bars
201 (Fig. 4). The lower rates were derived in a lower pH scenario, thus confirming that this is not an impact from pH. It
202 demonstrates that the non-ionic PAM slows down the calcite dissolution rate. Although the differences in pH are very
203 small, the data suggest an adverse impact of PAM on calcite dissolution and pore generation.

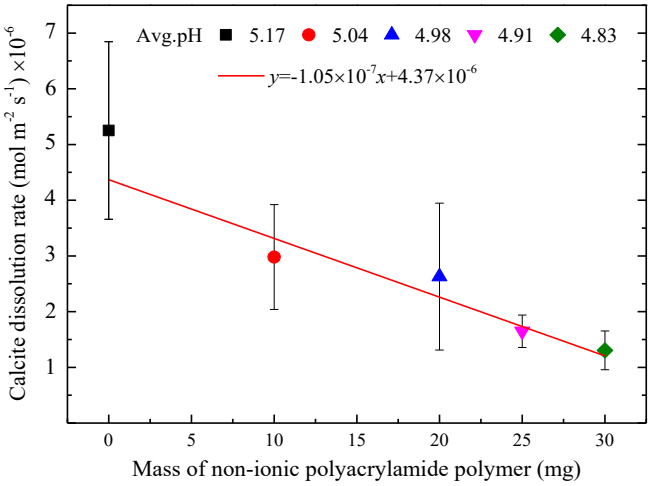

Fig. 4. Variation of calcite dissolution rate ($mol \cdot m^{-2} \cdot s^{-1}$) versus mass of non-ionic PAM polymer (mg).

4 Discussion

The addition of non-ionic PAM has resulted in a decrease in the dissolution rate of calcite (Fig. 4). We interpreted that the adsorption of the polymer onto the calcite surface slows down the dissolution of calcite. In the 0 mg polymer experiment, the calcite powder uniformly dispersed and a cloudy solution was then observed (Fig. 5a). When the calcite powder was added to a non-ionic PAM-containing solution, the aggregation of calcite powder was clearly seen, and the solution remained clear (Fig. 5b). The aggregation of calcite powder occurred regardless of the amount of non-ionic PAM (10-30 mg), however, a slightly lesser extent could be expected for a smaller amount of polymer in the experiments. We highly speculated that bridging adsorption would occur if there is some affinity between polymer segments and a particle surface (e.g. hydrogen bonding) (Bolto and Gregory, 2007). Bridging between two or more particles in the presence of polymer (Kim and Palomino, 2009) is potentially responsible for the aggregation of solid particles (Fig. 5b).

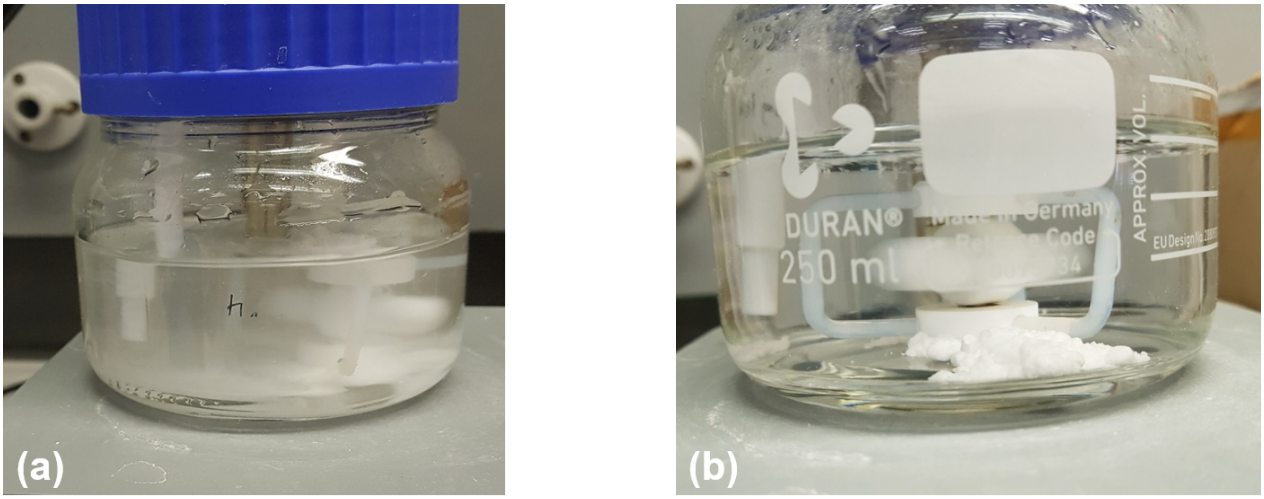

Fig. 5. Photographs of dispersed calcite powder in different buffer solutions: (a) 0 mg polymer experiment; (b) non-ionic PAM-containing experiment.

The adsorption of polymer onto calcite is highly likely through hydrogen bonding (Wang et al., 2017). The hydrogen

bonding occurs between the hydrogen atoms on the amide groups (a hydrogen donor) and oxygen atoms on the surface of the calcite. In neutral state, nitrogen forms three bonds and maintains one pair of non-bonded electrons. The 'carbonyl group' is part of non-ionic PAM (Fig. 6). The strong electron withdrawing nature of the carbonyl group (C=O) allows potential delocalisation, thus enabling the movement of non-bonded electrons of nitrogen into the adjacent carbonyl group (DeRuiter, 2005). The electron density is then pulled towards the oxygen and away from the hydrogen at the end of the group. This means the hydrogens in amide group will have a stronger positive dipole moment, thus enhancing the adsorption of PAM onto calcite surface (compared to water). Furthermore, the bound water on calcite surfaces enables two types of surface sites ($>CaOH^0$ and $>CO_3H^0$, where $>$ stands for the surface) (Van Capellen et al., 1993), and these sites were validated by spectroscopic data (Stipp, 1991). In a low pH scenario, the $>CaOH$ site may react with H^+ to form $>Ca(OH_2)^+$, which is the hydrated form of the $>Ca^+$ site (Geffroy et al., 1999). Moreover, the dangling amide group of the PAM polymer could be hydrolysed to form a carboxylic group (-COO-) (Ma et al., 2015). We speculated that the adsorption of PAM could also occur via the binding of carboxylate onto the surface site of $>Ca^+$ on calcite surface. Hence, surface complexation induced adsorption is also a possible way that can prevent calcite from dissolving. These findings may have implications in hydraulic fracturing in calcite-bearing shale reservoirs.

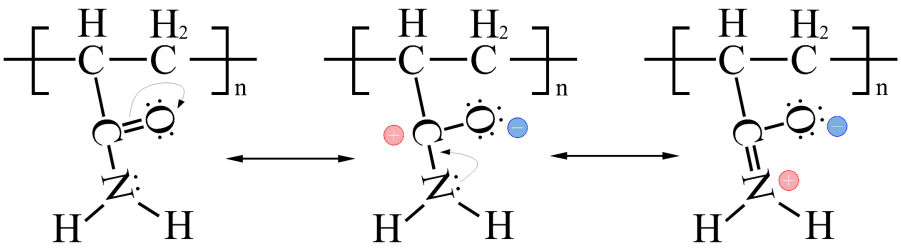

Fig. 6. Schematic of electron delocalization in an amide functional group (revised after DeRuiter, 2005).

Moreover, the dissolution rate of calcite obtained at 25 °C (Plummer and Wigley, 1976; Busenberg and Plummer, 1986; Chou et al., 1989) and room temperature (Shiraki et al., 2000) is very similar to the rates in this study for pH around 5 (Fig. 7). However, in situ dissolution rates of calcite at pH 5 were 10 times slower than those calculated in the laboratory (Fig. 7). This rate inhibition could be explained by the presence of external ions (Wicks and Groves, 1993).

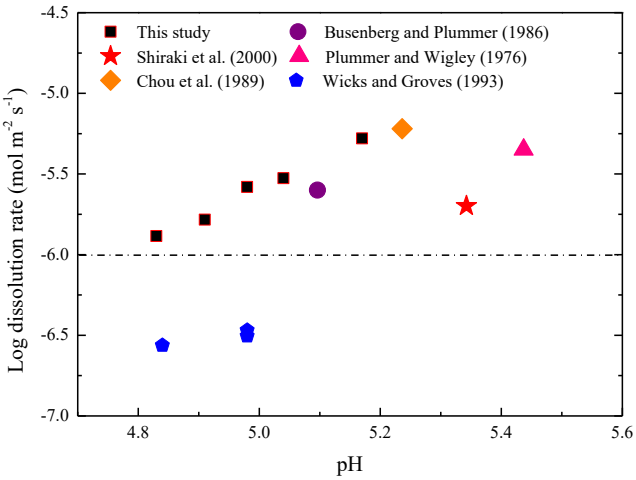

Fig. 7. Logarithm of calcite dissolution rate versus pH for this study and comparison with data from other studies on calcite dissolution.

At field sites, the adsorbed PAM also remains in the fracture network, thus decreasing the permeability of shale and posing an adverse impact on gas production (Grattoni et al., 2004; Carman and Cawiezel; Koteeswaran et al., 2017; Sun et al., 2017; Guo et al., 2018). Hence, PAM polymer not only retards calcite dissolution and pore generation (as discussed in section 3.2), but it also causes formation damage (decreased permeability). If the dissolution is inhibited to a certain extent, this can have a negative impact on fracture initiation and thus decrease conduit connectivity (permeability) in the reservoirs. In order to minimise the negative impacts of PAM on calcite dissolution and formation damage, practical measures which can degrade the polymer and/or prevent the polymer from adsorbing on calcite could enable enhanced recovery of unconventional gas.

Kot et al. (2012) incorporated temperature-sensitive azo groups in the polymer backbone, and this makes polymer more degradable at high temperature and results in less formation damage. Sun et al. (2011) developed a liquid emulsion form friction reducer, and it degrades more quickly than convention friction reducers at typical formation temperature. In addition, urea preferentially forms hydrogen bonds between itself and polymer (Wang et al., 2005), and thus reduced the adsorbed amount of polymer onto calcite surface in solution (Wang et al., 2017). Urea can remove the adsorbed amount of PAM on calcite surface and recover the permeability up to 72.46% (Li et al., 2018). Hence, degradable polymers and urea may potentially reduce the residue polymer onto calcite surface and promote the dissolution of calcite and gas recovery during fracturing activities.

Conclusions

Batch experiments were carried out to evaluate the calcite dissolution rate in a series of simulated fracturing fluids with different non-ionic PAM mass. The dissolution rate of calcite in the solution decreases from 5.3×10^{-6} $mol\cdot m^{-2}\cdot s^{-1}$ to 1.3×10^{-6} $mol\cdot m^{-2}\cdot s^{-1}$ as the amount of polymer increases from 0 mg to 30 mg, and thus demonstrates that the non-ionic PAM based friction reducer retards calcite dissolution. This finding shows the negative implications of non-ionic

PAM on fracture initiation and connectivity of the fracture networks during fracturing operations (e.g. negative implication for permeability of carbonate-bearing shale reservoirs), and thus decreasing the hydraulic fracturing efficiency and the productivity potential of unconventional hydrocarbon resources. This effect is potentially driven by hydrogen bonding and surface complexation induced adsorption of non-ionic PAM on calcite, thus slowing down calcite dissolution.

Appendix A. Experimental apparatus

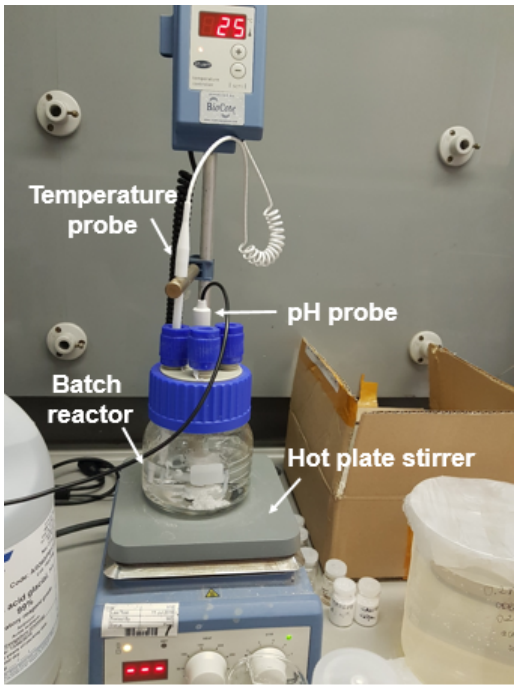

Fig. A.1 Photograph that shows the experimental appratus for the batch experiments.

Appendix B. Variation in specific surface area during ongoing dissolution of calcite

The geometric surface area A_{geom} is approximated by the assumption that the particles are smooth spheres with surface area and mass, based on an effective spherical diameter d_e and the calcite density ρ (Tester et al., 1994):

$$A_{geom} = \frac{\pi d_e^2}{\frac{4}{3}\pi(\frac{d_e}{2})^3 \rho} = \frac{\pi d_e^2}{(\pi/6) d_e^3 \rho} = \frac{6}{d_e \rho} \quad \text{(B.1)}$$

where ρ is 2.71 g/cm^3 and d_e is calculated based on the maximum (d_{max}) and minimum (d_{min}) particles size obtained from sieve sizes (d_{min} and d_{max} are 63 and 125 μm) in accordance with the following expression (Tester et al., 1994):

$$d_e = \frac{d_{max} - d_{min}}{\ln(\frac{d_{max}}{d_{min}})} \quad \text{(B.2)}$$

Since the measured surface area is larger than the calculated geometric area, a roughness factor ξ is therefore introduced to link the geometric surface area with the measured specific surface area of the calcite particles:

$$\xi = \frac{A_{bet}}{A_{geom}} \quad \text{(B.3)}$$

where A_{bet} is the specific surface area of the original calcite and equals 0.2615±10% $m^2 \cdot g^{-1}$.

The total volume of particles (particle size ranges from 63 to 125 μm) is calculated using the relationship between mass m and density. The total number of calcite particles N_c is approximately obtained by dividing the total volume by the volume of a single particle:

$$N_c = \frac{m/\rho}{\frac{4}{3}\pi(\frac{d_e}{2})^3} \quad \text{(B.4)}$$

During the dissolution of calcite, the decreasing particle size d_c can be defined as:

$$d_c = 2 \times (\frac{3m_r}{4\pi\rho N_c})^{\frac{1}{3}} \quad \text{(B.5)}$$

where m_r denotes the remaining calcite in the experiment at a specific time.

Therefore, the variation in the specific surface area of calcite is estimated as:

$$A_c = \frac{6\xi}{d_c\rho} = A_{bet}\frac{d_e}{d_c} \quad \text{(B.6)}$$

Based on the change in total calcite mass at each sampling step, we can then estimate the change in representative diameter, and based on this calculate the changing specific surface area using Eq. (B.6).

Acknowledgments

This research was funded by the Natural Environment Research Council (Grant NE/R018030/1) and the European Commission Horizon 2020 (grant number 764531). We thank Mark Guyler for maintenance of the ICP-OES in the School of Chemistry. We are grateful to the editor and two anonymous reviewers for their constructive comments, which helped to improve this manuscript.

References

Allain, J. P., Echeverry-Rendón, M., Surface treatment of metallic biomaterials in contact with blood to enhance hemocompatibility. In Hemocompatibility of Biomaterials for Clinical Applications; Elsevier, 2018.

Berner, R. A., Morse, J. W., 1974. Dissolution kinetics of calcium carbonate in seawater, IV. Theory of calcite dissolution. Am. J. Sci. 274, 108-134.

Busenberg, E., Plummer, L.N., 1986. A comparative study of the dissolution and crystal growth kinetics of calcite and aragonite. In: Mumptom, F.A. (Ed.), Studies Diagenesis, U.S.G.S. Bull., vol. 1578. U.S. Department of the Interior, Reston, pp. 139-168.

Brown, C. A., Compton, R. G., Narramore, C. A., 1993. The kinetics of calcite dissolution/precipitation. J. Colloid. Interf. Sci. 160(2), 372-

379.

Bolto, B., Gregory, J., 2007. Organic polyelectrolytes in water treatment. Water. Res. 41, 2301-2324.

Britt, L., 2012. Fracture stimulation fundamentals. J. Nat. Gas. Sci. Eng. 8, 34-51.

Chou, L., Garrels, R. M., Wollast, R., 1989. Comparative study of the kinetics and mechanisms of dissolution of carbonate minerals. Chem. Geol. 78(3-4), 269-282.

Compton, R. G., Brown, C. A., 1994. The inhibition of calcite dissolution/precipitation: Mg^{2+} cations. J. Colloid. Interf. Sci. 165(2), 445-449.

Cubillas, P., Köhler, S., Prieto, M., Chaïrat, C., Oelkers, E. H., 2005. Experimental determination of the dissolution rates of calcite, aragonite, and bivalves. Chem. Geol. 216, 59-77.

Carman, P. S., Cawiezel, K. E., 2007. Successful breaker optimization for polyacrylamide friction reducers used in slickwater fracturing. In: SPE hydraulic fracturing technology conference. College Station, Texas: Society of Petroleum Engineers.

Chalmers, G. R. L., Ross, D. J. K., Bustin, R. M., 2012. Geological controls on matrix permeability of Devonian Gas Shales in the Horn River and Liard basins, northeastern British Columbia, Canada. Int. J. Coal. Geol. 103, 120-131.

Dolgaleva, I. V., Gorichev, I. G., Izotov, A. D., Stepanov, V. M., 2005. Modeling of the effect of pH on the calcite dissolution kinetics. Theor. Found. Chem. Eng. 39, 614-621.

DeRuiter, J., 2005. Amides and related functional groups. Principles of Drug Action 1.

De Baere, B., Molins, S., Mayer, K. U., François, R., 2016. Determination of mineral dissolution regimes using flow-through time-resolved analysis (FT-TRA) and numerical simulation. Chem. Geol. 430, 1-12.

Fredd, C. N., Fogler, H. S., 1998. The kinetics of calcite dissolution in acetic acid solutions. Chem. Eng. Sci. 53(22). 3863-3874.

Ferrer, I., Thurman, E. M., 2015. Chemical constituents and analytical approaches for hydraulic fracturing waters. Trends. Environ. Anal. 5, 18-25.

Farhang, F., Rayson, M., Brent, G., Hodgins, T., Stockenhuber, M., Kennedy, E., 2017. Insights into the dissolution kinetics of thermally activated serpentine for CO2 sequestration. Chem. Eng. J. 330, 1174-1186.

Geffroy, C., Foissy, A., Persello, J., Cabane, B., 1999. Surface complexation of calcite by carboxylates in water. J. Colloid. Interface. Sci. 211, 45-53.

Grattoni, C. A., Luckham, P. F., Jing, X. D., Norman, L., Zimmerman, R. W., 2004. Polymers as relative permeability modifiers: adsorption and the dynamic formation of thick polyacrylamide layers. J. Petrol. Sci. Eng. 45, 233-245.

Gong, Q., Deng, J., Wang, Q., Yang, L., She, M., 2008. Calcite dissolution in deionized water from 50 °C to 250 °C at 10 MPa: rate equation and reaction order. Acta. Geol. Sin. 82(5), 994-1001.

Gouze, P., Luquot, L., 2011. X-ray microtomography characterization of porosity, permeability and reactive surface changes during dissolution. J. Contam. Hydrol. 120-121, 45-55.

Gregory, K. B., Vidic, R. D., Dzombak, D. A., 2011. Water management challenges associated with the production of shale gas by hydraulic fracturing. Elements 7, 181-186.

Gordalla, B. C., Ewers, U., Frimmel, F. H., 2013. Hydraulic fracturing: a toxicological threat for groundwater and drinking-water? Environ. Earth. Sci. 70, 3875-3893.

Guo, T., Li, Y., Ding, Y., Qu, Z., Gai, N., Rui, Z., 2017. Evaluation of acid fracturing treatments in shale formation. Energy Fuels 31, 10479-

340 10489.
341 Guo, J., Li, Y., Wang, S., 2018. Adsorption damage and control measures of slick-water fracturing fluid in shale reservoirs. Petrol. Explor.
342 Dev. 45(2), 336-342.
343 Geri, M. B., Imqam, A., Flori, R., 2019. A critical review of using high viscosity friction reducers as fracturing fluids for hydraulic fracturing
344 applications. In: Presented at the SPE Oklahoma City Oil and Gas Symposium. Society of Petroleum Engineers.
345 Holdren Jr, G. R., Berner, R. A., 1979. Mechanism of feldspar weathering-I. Experimental studies. Geochim. Cosmochim. Acta. 43, 1161-
346 1171.
347 Hammack, R. W., Harbert, W., Sharma, S., Stewart, B. W., Capo, R. C., Wall, A. J., Wells, A., Diehl, R., Blaushild, D., Sams, J., Veloski, G.,
348 2014. An Evaluation of Fracture Growth and Gas/Fluid Migration as Horizontal Marcellus Shale Gas Wells Are Hydraulically Fractured
349 in Greene County, Pennsylvania; Report NETL-TRS-3−2014; U.S. Department of Energy, National Energy Technology Laboratory:
350 Pittsburgh, PA.
351 Habibpour, M., Clark, P. E., 2017. Drag reduction behaviour of hydrolysed polyacrylamide/xanthan gum mixed polymer solutions. Pet. Sci.
352 14, 412-423.
353 Konhauser, K., 2007. Introduction to geomicrobiology. Blackwell Publishing, Oxford.
354 Kim, S., Palomino, A. M., 2009. Polyacrylamide-treated kaolin: A fabric study. Appl. Clay. Sci. 45, 270-279.
355 King, G. E., 2012. Hydraulic Fracturing 101: What Every Representative, Environmentalists, Regulator, Reporter, Investor, University
356 Researcher, Neighbor and Engineer Should Know About Estimating Frac Risk and Improving Frac Performance in Unconventional Gas
357 and Oil Wells. Paper presented at SPE Hydraulic Fracturing Technology Conference, The Woodlands, Texas.
358 Kharisov, R. Y., Folomeev, A. E., Sharifullin, A. R., Bulgakova, G. T., Telin, A. G., 2012. Integrated approach to acid treatment optimization
359 in carbonate reservoirs. Energy Fuels 26, 2621-2630.
360 Kot, E., Saini, R., Norman, L. R., Bismarck, A., 2012. Novel drag-reducing agents for fracturing treatments based on polyacrylamide
361 containing weak labile links in the polymer backbone. SPE. J. 17(03), 924-930.
362 Koteeswaran, S., Pashin, J. C., Ramsey, J. D., Clark, P. E., 2017. Quantitative characterization of polyacrylamide–shale interaction under
363 various saline conditions. Pet. Sci. 14, 586-596.
364 Li, Y., Wang, S., Guo, J., Gou, X., Jiang, Z., Pan, B., 2018. Reduced adsorption of polyacrylamide-based fracturing fluid on shale rock using
365 urea. Energy. Sci. Eng. 6, 749-759.
366 Mohan, C., 2003. Buffers: A guide for the preparation and use of buffers in biological systems. EMD Biosciences Inc., San Diego, Caifornia.
367 Morsy, S., Sheng, J. J., Hetherington, C. J., Soliman, M. Y., Ezewu, R. O., 2013. Impact of matrix acidizing on shale formations. In: Paper
368 SPE 167568 Presented at the Nigeria Annual International Conference and Exhibition Held in Lagos, Nigeria.
369 Ma, Q., Shuler, P.J., Aften, C.W., Tang, Y., 2015. Theoretical studies of hydrolysis and stability of polyacrylamide polymers. Polym. Degrad.
370 Stab. 121, 69-77.
371 Motiee, M., Johnson, M., Ward, B., Gradl, C., McKimmy, M., Meeheib, J., 2016. High Concentration Polyacrylamide-Based Friction Reducer
372 Used as a Direct Substitute for Guar-Based Borate Crosslinked Fluid in Fracturing Operations. In: Proc., SPE Hydraulic
373 FracturingTechnology Conference, the Woodlands, Texas, USA.
374 Nguyen, T. C., Romero, B., Vinson, E., Wiggins, H., 2018. Effects of salt on the performance of drag reducers in slickwater fracturing fluids.

375 J. Petrol. Sci. Eng. 163, 590-599.
376 Plummer, L. N., Wigley, T. M. L., 1976. The dissolution of calcite on CO2-saturated solutions at 25 °C and 1 atmosphere total pressure.
377 Geochim. Cosmochim. Acta. 40, 191-201.
378 Plummer, L.N., Wigley, T.M.L., Parkhurst, D.L., 1978. The kinetics of calcite dissolution in CO2-water systems at 5 degrees to 60 degrees
379 and 0.0 to 1.0 atm CO2. Am. J. Sci. 278, 179-216.
380 Pracný, P., Faimon, J., Všianský, D., Přichystala, A., 2019. Evolution of Mg/Ca and Sr/Ca ratios during the experimental dissolution of
381 limestone. Chem. Geol. 523, 107-120.
382 Renard, F., Bernard, D., Desrues, J., Ougier-Simonin, A., 2009. 3D imaging of fracture propagation using synchrotron X-ray
383 microtomography. Earth. Planet. Sci. Lett. 286, 285-291.
384 Rimassa, S. M., Howard, P. R., Arnold, M. O., 2009. Are you buying too much friction reducer because of your biocide? In: SPE hydraulic
385 fracturing technology conference,Soc Pet Eng, Texas, USA: The Woodlands.
386 Roncal-Herrero, T., Oelkers, E. H., 2011. Does variscite control phosphate availability in acidic natural waters? An experimental study of
387 variscite dissolution rates. Geochim. Cosmochim. Acta. 75, 416-426.
388 Rodvelt, G., Yuyi, S., VanGilder, C., 2015. Use of a salt-tolerant friction reducer improves production in Utica completions. In SPE Eastern
389 Regional Meeting. Society of Petroleum Engineers, Richardson, TX.
390 Shaw, D. B., Weaver, C. E., 1965. The mineralogical composition of shales. J. Sediment. Res. 35(1), 213-222.
391 Sjöberg, E. L., 1976. A fundamental equation for calcite dissolution kinetics. Geochim. Cosmochim. Acta. 40, 441-447.
392 Sjöberg, E. L., Rickard, D. T., 1984. Temperature dependence of calcite dissolution kinetics between 1 and 62 C at pH 2.7 to 8.4 in aqueous
393 solutions. Geochim. Cosmochim. Acta. 48(3), 485-493.
394 Stipp, S., Hochella Jr., M.F., 1991. Structure and bonding environments at the calcite surface as observed with X-ray photo-electron
395 spectroscopy (XPS) and low energy electron diffraction (LEED). Geochim. Cosmochim. Acta. 55, 1723-1736.
396 Shiraki, R., Rock, P. A., Casey, W. H., 2000. Dissolution kinetics of calcite in 0.1 M NaCl solution at room temperature: an atomic force
397 microscopic (AFM) study. Aquat. Geochem. 6, 87-108.
398 Sun, H., Stevens, D., Cutler, J., Cutler, J., Wood, B., Wheeler, R., 2011. A novel nondamaging friction reducer: development and successful
399 slickwater frac applications. SPE Hydraulic Fracturing Technology Conference, the Woodlands, Texas, USA.
400 Slatt, R. M., 2013. Chapter 12-Unconventional resource shales. Dev. Pet. Sci. 61, 553–620.
401 Sun, Y., 2014. Impact of slickwater fracturing fluid compositions on the petrophysical properties of shale and tight sand. Ph.D. Dissertation,
402 Missouri University of Science and Technology: Rolla, MO.
403 Sun, Y., Bai, B., Ma, Y., Jr, R. F., 2014. Flow behavior characterization of a polyacrylamide-based friction reducer in microchannels. Ind.
404 Eng. Chem. Res. 53, 20036–20043.
405 Sun, Y., Bai, B., Dai, C., Liu, H., 2017. Permeability evolution study after breaking of friction reducer in near fracture matrix of tight gas
406 reservoir. Fuel. 204, 63-70.
407 Shovkun, I., Espinoza, D. N., 2017. Shale acid fracturing: geomechanical effects and fracture propagation. Poromechanics VI, 1924-1929.
408 Sulpis, O., Mucci, A., Boudreau, B. P., Barry, M. A., Johnson, B. D., 2019. Controlling the diffusive boundary layer thickness above the
409 sediment-water interface in a thermostated rotating-disk reactor. Limnol. Oceanogr.:Methods. 17, 241-253.

Tester, J. W., Worley, W. G., Robinson, B. A., Grigsby, C. O., Feerer, J. L., 1994. Correlating quartz dissolution kinetics in pure water from 25 to 625 °C. Geochim. Cosmochim. Acta. 58(11), 2407-2420.

Van Capellen, P., Charlet, L., Stumm, W., Wersin, P., 1993. A surface complexation model of the carbonate mineral-aqueous solution interface. Geochim. Cosmochim. Acta. 57, 3505-3518.

Vidic, R. D., Brantley, S. L., Vandenbossche, J. M., Yoxtheimer, D., Abad, J. D, 2013. Impact of Shale Gas Development on Regional Water Quality. Science 340(6134), 1235009.

Wicks, C. M., Groves, C. G., 1993. Acidic mine drainage in carbonate terrains: geochemical processes and rates of calcite dissolution. J. Hydrol. 146, 13-27.

Wang, J., Somasundaran, P., Nagaraj, D. R., 2005. Adsorption mechanism of guar gum at solid-liquid interfaces. Miner. Eng. 18, 77-81.

Wolff-Boenisch, D., Traina, S. J., 2007. The effect of desferrioxamine B, enterobactin, oxalic acid, and Na-alginate on the dissolution of uranyl-treated goethite at pH 6 and 25 °C. Chem. Geol. 243, 357-368.

Wang, S., Li, G., Li, Y., Guo, J., Zhou, S., Yong, S., Pan, B., Bai, B., 2017. Adsorption of new hydrophobic polyacrylamide on the calcite surface. J. Appl. Polym. Sci. 134(38), 45314.

Wu, W., Sharma, M. M., 2015. Acid fracturing shales: effect of dilute acid on properties and pore structure of shale. Proceedings of the Society of Petroleum Engineers (SPE) Hydraulic Fracturing Technology Conference; The Woodlands, Texas.

Xiong, B., Loss, R. D., Shields, D., Pawlik, T., Hochreiter, R., Zydney, A. L., Kumar, M., 2018a. Polyacrylamide degradation and its implications in environmental systems. Clean Water 1(1), 17.

Xiong, B., Miller, Z., Roman-White, S., Tasker, T., Farina, B., Piechowicz, B., Burgos, W. D., Joshi, P., Zhu, L., Gorski, C. A., Zydney, A. L., Kumar, M., 2018b. Chemical degradation of polyacrylamide during hydraulic fracturing. Environ. Sci. Technol. 52, 327-336.

Yang, B., Zhao, J., Mao, J., Tan, H., Zhang, Y., Song, Z., 2019. Review of friction reducers used in slickwater fracturing fluids for shale gas reservoirs. J. Nat. Gas. Sci. Eng. 62, 302-313.

Zou, Y., Li, S., Ma, X., Zhang, S., Li, N., Chen, M., 2018. Effects of CO2–brine–rock interaction on porosity/permeability and mechanical properties during supercritical-CO2 fracturing in shale reservoirs. J. Nat. Gas. Sci. Eng. 49, 157-168.

List of Figures

List of Tables

Table 1 Average calcite dissolution rates calculated based on the experiments with non-ionic PAM containing-solution. The pH value is the average pH (± stdev) calculated from six pH measurements (30-80 min) in the experiment used to calculate the calcite dissolution rate.